POLITECNICO
MILANO 1863

SCUOLA DI INGEGNERIA INDUSTRIALE
E DELL'INFORMAZIONE

Executive Summary of the Thesis

Method Development for Poisson's Ratio Determination in Cartilage Using Fibril-Reinforced Models

Laurea Magistrale in Biomedical Engineering - Ingegneria Biomedica

Author: Marco Sartorio

Advisors: Viktor Jönsson, Hanna Isaksson, Emiliano Votta

Academic year: 2024-2025

1. Introduction

Knee osteoarthritis (OA) is the most common pathology affecting the knee joint, resulting in severe damage to the whole joint, including progressive loss of articular cartilage (AC). As the mechanisms behind OA are not fully understood, preventive efforts are mostly restricted to addressing modifiable risk factors such as obesity and prior injuries. From a mechanical perspective, AC is commonly described as a biphasic material consisting of a solid and fluid phase. In fibril-reinforced constitutive models, the solid phase is typically decomposed into a fibrillar component, representing the collagen network, and a non-fibrillar component, representing the proteoglycan-rich matrix. Within these formulations, the non-fibrillar Poisson ratio is a material parameter governing the deformation behavior of the solid matrix. In AC experimental studies, Poisson ratio is commonly estimated from optical measurements; however, this provides an apparent value that reflects the overall macroscopic response of the tissue and therefore cannot be directly used to describe the non-fibrillar matrix. Despite its explicit presence in these formulations, non-fibrillar Poisson ratio has not been systematically investigated in the literature and is often assumed, potentially leading to inaccurate predictions of the mechanical response of the tissue. Moreover, OA progression alters collagen architecture, proteoglycan content, and water distribution, resulting in well-known changes in cartilage stiffness and permeability. Conversely, the literature addressing Poisson ratio in osteoarthritic cartilage remains limited. Predictive knee joint models for OA currently assume a constant Poisson ratio, while other mechanical properties change in the models, and its implications on joint mechanics have not been systematically assessed. Therefore, the development of a method for non-fibrillar Poisson ratio determination in AC is crucial to improve the reliability and predictive capability of patient-specific knee joint models.

2. Materials and Methods

2.1. Experimental data

The experimental dataset was acquired as part of a proof-of-concept study performed at the TOMCAT beamline (Swiss Light Source, Paul Scherrer Institute, Switzerland [1]) by the Lund Biomechanics research group, prior to the beginning of this thesis work. Eight cylindrical healthy bovine AC samples (4 mm diameter) were harvested from the femoropatellar groove. Time-resolved synchrotron-based X-ray phase-

contrast micro-computed tomography (SR-PhC-μCT) was used to investigate tissue behavior under mechanical loading. Unconfined compression with a stress-relaxation protocol was employed to test the samples. After preloading to ensure proper contact, two displacement-controlled compression steps (15% strain each) were applied, with relaxation phases to capture time-dependent behavior. Force-time curves were recorded and both dynamic and static scans were acquired throughout the test (Figure 1).

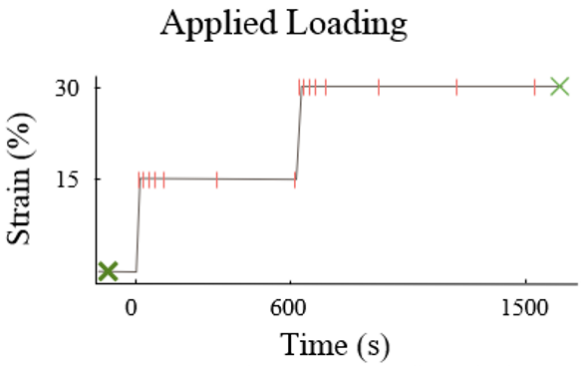

Figure 1: Schematic of the stress-relaxation protocol used for AC samples testing. Green crosses indicate static scans, while red bars represent dynamic scans.

2.2. Image data

Since parameter identification was the primary aim of the present analysis, the selection of the specimens included in the workflow was based on the following criteria: (i) presence or absence of calcified cartilage and subchondral bone, (ii) irregular geometry or macroscopic defects (e.g, missing cartilage), and (iii) correct adherence to the loading plate during mechanical testing. Previous work has shown that both residual calcified tissue and geometric imperfections consistently affect the mechanical response of AC in unconfined compression, introducing variability unrelated to the intrinsic material properties and potentially biasing parameter estimation [3]. Tomographic datasets were therefore analyzed in ImageJ, leading to the selection of two suitable samples for further analysis. Representative images of both samples in their unloaded configurations are provided in Figure 2, while dynamic images of sample 02 at 15% and 30% strain are presented in Figure 3.

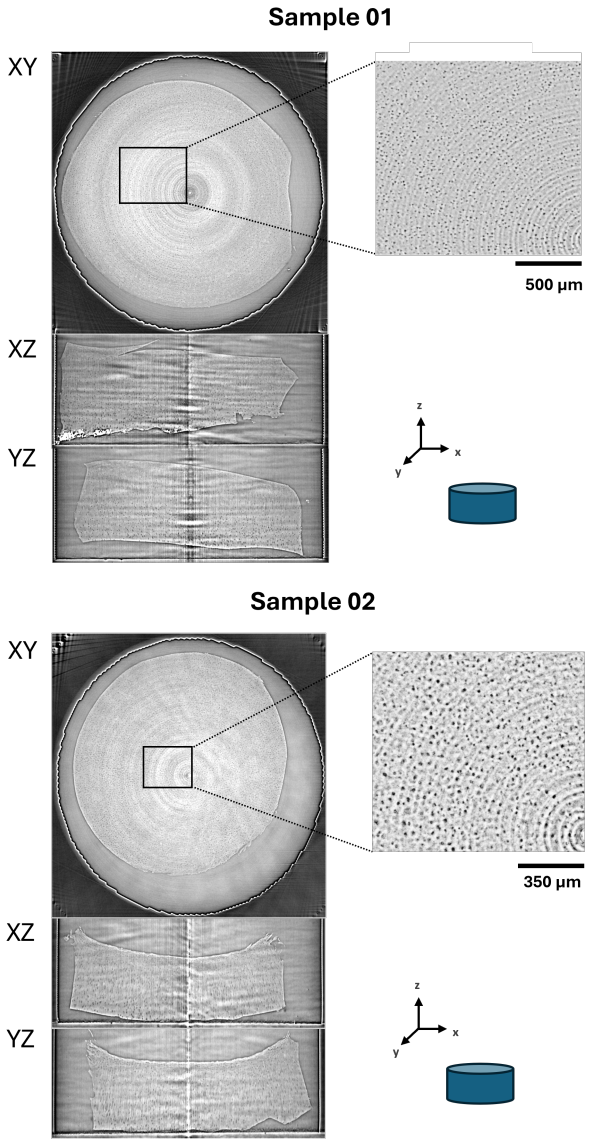

Figure 2: Orthogonal static views (XY, XZ, YZ planes) of sample 01 and 02. Two enlarged insets are provided to improve the visualization of chondrocytes.

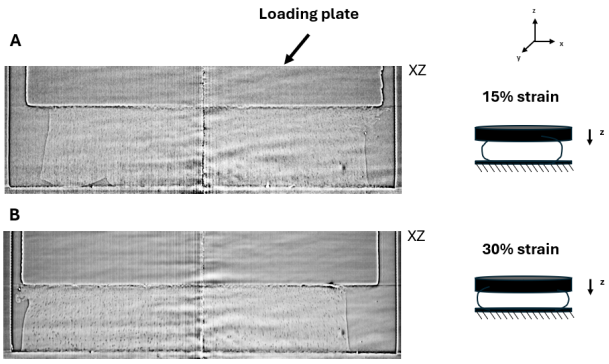

Figure 3: XZ orthogonal dynamic views showing the response of sample 02 after 15% and 30% compression.

The lateral expansion under compression was evaluated by measuring the cross-sectional area from top-view (XY-plane) images at three key time points: the initial undeformed configuration and two equilibrium deformed conditions after 15% and 30% strain. For each configuration, a representative central region of the sample was segmented in ImageJ, and the averaged cross-sectional area was used to quantify lateral deformation.

2.3. Idealized FE model

Two idealized cylindrical FE models of AC (4 mm diameter; heights: 1.39 mm and 1.01 mm) were developed. A fibril-reinforced poroHyperelastic (FRPE) material model was assigned as a user-defined material in ABAQUS/Standard (Version 2023, SIMULIA, Dassault Systèmes). The porous non-fibrillar matrix was modeled as a compressible Neo-Hookean material, while the fibrillar network consisted of depth-dependent collagen fibrils oriented according to the Benninghoff arcade model. Fluid flow was governed by Darcy's law with strain-dependent permeability. The models were discretized using 8-nodes poroelastic hexaedral elements (C3D8P) with characteristic dimensions of 0.18 mm and 0.25 mm, which were set upon mesh convergence analysis. Boundary conditions were assigned to prevent rigid body motion without restricting radial expansion, in order to reproduce the testing protocol. Free fluid flow (e.g, null pore pressure) was allowed through the lateral surfaces, while the top and bottom surfaces were assumed to be impermeable. The load was displacement-controlled and applied to the top surface (Figure 4).

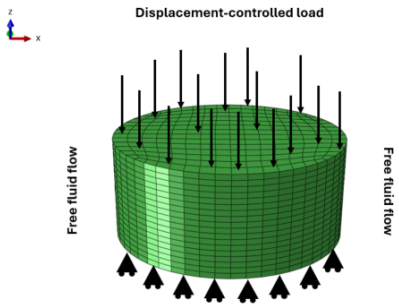

Figure 4: Idealized FE model and boundary conditions.

2.4. Material properties

The FRPE material model adopted in this study is described by seven parameters: the Young's modulus of the non-fibrillar matrix E_{nf}, its Poisson ratio ν_{nf}, the Young's moduli of the linear and non-linear fibrillar components E_0 and E_{fe}, respectively, the initial permeability K_0, the strain-dependent permeability exponent M, and the ratio between primary and secondary collagen fibrils C. All material parameters, except for C, were identified by fitting the model to the experimental data to allow the estimation of ν_{nf}, while also optimizing the remaining parameters. The fitting pipeline developed in this work simultaneously minimized the error in the reaction force and lateral expansion (quantified through areal strain), enabling to capture both the axial and transverse responses of AC.

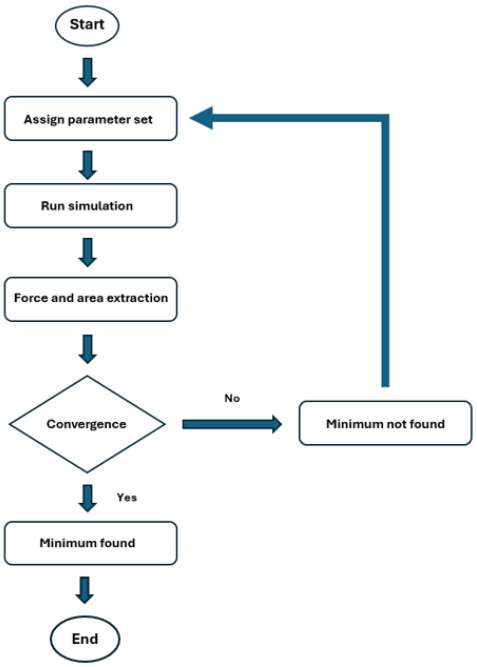

Figure 5: Fitting workflow corresponding to a single restart of the GBNM-based routine. A new initial guess is automatically generated after convergence, resulting in a continuous loop.

An automated optimization routine was implemented as an iterative process that combines MATLAB and ABAQUS. For each parameter set, the FE simulation of the unconfined compression test was run, reaction forces and lateral expansion were extracted, and a weighted error function combining force and strain contributions was evaluated ($RMSE_{tot}$). The ma-

terial parameters were iteratively updated until convergence was achieved. The minimization of $RMSE_{tot}$ was implemented through the Globalized-Bounded Nelder-Mead (GBNM) algorithm, which automatically restarts the optimization with a new unique initial guess once a local minimum is reached (Figure 5).

2.5. Sample-specific model

A sample-specific FE model was developed for specimen 02 to assess the influence of realistic geometry on parameter fitting, as the corresponding cylindrical model showed deviations from the experimental behavior. Tomographic images were semi-automatically segmented using open-source software 3D Slicer and Seg3D. The reconstructed geometry was discretized in ANSA v24.1.2 (BETA CAE) into linear tetrahedral elements (0.15 mm characteristic dimension, set upon convergence analysis), and imported into ABAQUS as C3D4P elements for coupled pore-pressure analysis. The sample was positioned between two rigid plates with frictionless contact, where the upper plate was prescribed a vertical downward displacement and the lower plate was fully constrained. To prevent rigid body motion while allowing for lateral expansion, the same strategy applied in the idealized model was used. In order to fit the material parameters on the experimental data, the developed optimization pipeline was applied.

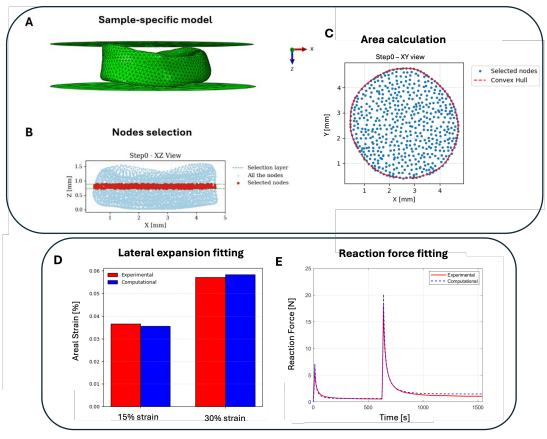

Figure 6: Overview of the sample-specific model and fitting procedure. A) 3D geometry (sample 02). B) XZ view showing the nodes selection process. C) XY view describing the area calculation method. D) Example of lateral expansion fitting. E) Example of reaction force fitting.

3. Results

3.1. Areal strain evaluation

The total lateral expansion over the full stress-relaxation protocol reached 5.7% for sample 01 and 7.4% for sample 02, corresponding to an average of 6.6% (Table 1).

Step	Sample 01	Sample 02
1st step	+3.66%	+3.37%
2nd step	+2.05%	+3.89%
Total expansion	**+5.71%**	**+7.38%**

Table 1: Lateral expansion (%) from μCT images for the two samples.

.

3.2. Fitting of the idealized models

For sample 01, the idealized sample model with the identified constitutive parameters accurately reproduced the experimental response ($RMSE_{tot} = 0.084$), (Table 2, Figure 7A–B). The simulation with a sample-specific geometry was hence deemed unnecessary.

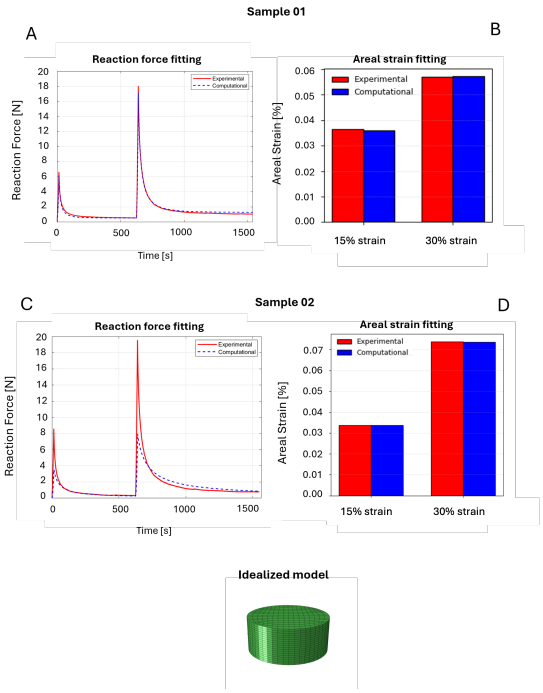

Figure 7: Results of the optimization for the idealized models of samples 01 and 02. A-B) Sample 01: reaction force (A) and lateral expansion fitting (B). C-D) Sample 02: reaction force (C) and lateral expansion fitting (D).

	E_0 (MPa)	E_{nf} (MPa)	ν_{nf} (–)	E_{fe} (MPa)	k_0 (mm^4/Ns)	M (–)
Idealized model (01)	0.12	0.063	0.46	271	0.010	6.83
Idealized model (02)	0.25	0.054	0.26	73	0.0057	8.16
Sample-specific model (02)	0.10	0.075	0.35	116	0.0091	5.85
Ebrahimi et al. [2]	0.86 ±0.46	0.29 ±0.15	0.42*	4.01 ±3.69	0.0037 ±0.0028	9.84 ±3.85
Julkunen et al. [4]	0.92 ±0.33	0.22 ±0.1	0.22*	150 ±113	0.006 ±0.0012	5.1 ±0.9

Table 2: Fitted FRPE material parameters for idealized and sample-specific models, with literature data for comparison [2, 4]. Values marked with * were fixed during the optimization. Note that Julkunen et al. employed a fibril-reinforced poroviscoelastic (FRPVE) material model.

In contrast, for sample 02 the idealized model with the identified constitutive parameters resulted in higher combined error ($RMSE_{tot} = 0.14$). While equilibrium forces were predicted with high accuracy, peak forces were substantially underestimated, exhibiting relative errors around 60%. Lateral expansion was predicted with similarly high accuracy as in sample 01, with negligible deviations from the experimental areal strain values (Figure 7C-D). Thus, further simulations were performed with the sample-specific geometry.

3.3. Fitting of the sample-specific model: sample 02

While the FRPE material model produced heterogeneous strain distributions due to its anisotropy, the idealized model exhibited a more homogeneous strain field than the sample-specific case. However, when the fitting was repeated using a sample-specific geometry for sample 02, the overall accuracy did not improve, exhibiting a $RMSE_{tot} = 0.16$ (Figure 8A-B).

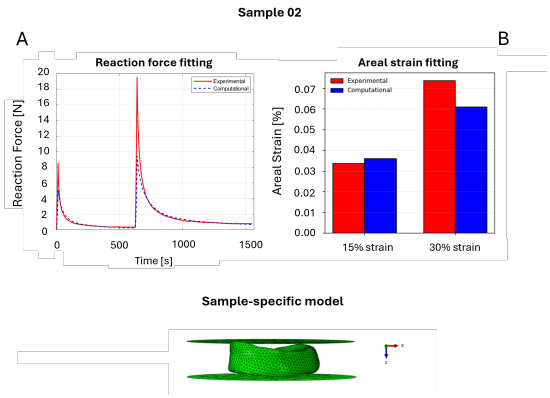

Figure 8: Results of the optimization for the sample-specific model of sample 02, showing the fitting of reaction force (A) and lateral expansion (B).

The reaction force profile showed a slight improvement compared to the idealized model. Equilibrium forces were predicted with high accuracy, whereas peak forces remained overestimated, although less markedly, with deviations by up to 51% for the second peak. In contrast, the prediction of lateral expansion worsened, reaching an overall discrepancy by approximately 15% after the second compression.

4. Discussion

A method for material parameter identification through FE simulation was developed and tested using synchrotron-based stress-relaxation data from AC samples. Unlike previous studies relying on static side views, this work leveraged high-resolution tomographic images to track areal strain under loading. The fitting included both reaction forces and lateral expansion, allowing the estimation of non-fibrillar Poisson ratio. In the idealized models, lateral expansion was well captured in both samples. While sample 01 showed a good fit between experimental and simulated reaction forces, sample 02 underpredicted peak forces. In healthy AC, axial compression induces lateral expansion that is limited by the collagen network, resulting in increased fluid pressure that primarily governs the instantaneous response of the tissue. The peaks underestimation therefore suggest that the constraining function of collagen network, and consequently, fluid pressurization, were not adequately captured. Although both samples were taken from the same bovine knee, they exhibited significant mechanical variability (up to 34% in equilibrium force and 30% in areal strain), leading to different optimization problems. In sample 02, fitting the higher experimental areal strain required reduced overall collagen

stiffness, resulting in lower peak forces. The fitting resulted in a lower initial permeability k_0 and a higher strain-dependent exponent M. Due to their coupled effects, different (k_0, M) combinations can produce similar macroscopic behaviors, limiting unique parameter identification. In this case, opposite trends were observed between the idealized models, preventing a clear interpretation of permeability-related effects on the peak response. In contrast, equilibrium forces were accurately captured in both idealized models. At equilibrium, fluid flow has ceased and permeability no longer influences the response. The equilibrium behavior is governed by the non-fibrillar matrix, whose fitted stiffness differed by only 15% between the two samples. The substantial decrease in non-fibrillar Poisson ratio ν_{nf} from sample 01 suggests parameter compensation within the model, rather than true material properties. Since the fitted collagen stiffness and permeability parameters could not simultaneously reproduce both peak forces and areal strain, ν_{nf} was shifted toward low values to match the lateral expansion data. Consequently, the parameters identified for sample 01 can be interpreted with greater confidence. To examine whether accounting for the actual geometry could improve the fitting accuracy, a sample-specific model was developed for sample 02, whose idealized configuration exhibited larger deviations from the experimental response. Although the reaction force profile showed an improvement, the total areal strain was underpredicted and the $RMSE_{tot}$ increased (0.16 vs 0.14). The additional spatial heterogeneities altered the local mechanical response, resulting in optimized parameter variations ranging from -60% to +60%, yet the global mechanical response remained comparable to the idealized case. Compensatory adjustments, most notably between E_0 and E_{fe}, as well as K_0 and M, produced minor improvements in fluid pressurization during the transient phases, but remained insufficient to reproduce the experimental peak forces. The increase in E_{nf} and ν_{nf} likely contributed to accurate equilibrium prediction, yet collagen constraints limited lateral expansion, leading to areal strain underestimation. Direct comparison of the fitted material parameters with literature is challenging due to differences in experimental protocol, biological source, material modeling, and fitting objectives. Indentation-based analyses [2] primarily engage superficial collagen fibrils, whereas unconfined compression predominantly loads deeper fibrils that strongly influence lateral expansion, resulting in different collagen network recruitment and load-bearing behavior. Species differences further complicate interpretation, as bovine cartilage generally exhibits higher stiffness than human tissue. Moreover, the adoption of fibril-reinforced poroviscoelastic (FRPVE) formulations in some studies [4] introduces intrinsic collagen viscosity, increasing the number of interacting parameters and modifying load redistribution during relaxation. Consequently, fibrillar and permeability-related parameters are not directly comparable. Within this framework, and particularly when areal strain is not included as a fitting target, the variations observed in Table 2 likely reflect differences in experimental protocols and constitutive formulations across studies.

5. Conclusions

This thesis explored the feasibility of estimating the non-fibrillar Poisson ratio of AC by simultaneously fitting axial and transverse mechanical responses. The integration of time-resolved synchrotron microCT imaging with FE modeling enabled direct quantification of lateral expansion, revealing mechanical features not captured when relying solely on axial force data. Overall, these findings provide a foundation for future studies aimed at identifying intrinsic cartilage properties and support the development of improved patient-specific computational joint models.

References

[1] Hector Dejea et al. *Advanced Science*, 2024.

[2] Mohammadhossein Ebrahimi et al. *Annals of Biomedical Engineering*, 2021.

[3] Viktor Jonsson et al. *Journal of Biomechanics*, 2024.

[4] Petro Julkunen et al. *Journal of Biomechanics*, 2007.